Geophysical Research Letters

RESEARCH LETTER
10.1029/2022GL101671

# Interannual Changes in Tidal Conversion Modulate $M_2$ Amplitudes in the Gulf of Maine

**Michael Schindelegger[1], Daniel P. Kotzian[1], Richard D. Ray[2], J. A. Mattias Green[3], and Sophie Stolzenberger[1]**

[1]Institute of Geodesy and Geoinformation, University of Bonn, Bonn, Germany, [2]Geodesy & Geophysics Laboratory, NASA Goddard Space Flight Center, Greenbelt, MD, USA, [3]School of Ocean Sciences, Bangor University, Menai Bridge, UK

**Key Points:**

- We propagate the $M_2$ tide through realistic, annually varying density structures (1993–2019) in a regional Gulf of Maine model
- Stratification changes explain 32%–48% of the observed, cm-level $M_2$ amplitude variability at coastal tide gauges from 1994 to 2019
- Modeled $M_2$ changes mainly reflect fluctuations in the barotropic-baroclinic energy conversion rate on the New England continental slope

**Supporting Information:**

Supporting Information may be found in the online version of this article.

**Correspondence to:**

M. Schindelegger,
schindelegger@igg.uni-bonn.de

**Citation:**

Schindelegger, M., Kotzian, D. P., Ray, R. D., Green, J. A. M., & Stolzenberger, S. (2022). Interannual changes in tidal conversion modulate $M_2$ amplitudes in the Gulf of Maine. *Geophysical Research Letters*, *49*, e2022GL101671. https://doi.org/10.1029/2022GL101671

Received 10 OCT 2022
Accepted 1 DEC 2022

**Author Contributions:**

**Conceptualization:** Michael Schindelegger, J. A. Mattias Green
**Data curation:** Michael Schindelegger, Daniel P. Kotzian
**Formal analysis:** Michael Schindelegger, Daniel P. Kotzian
**Funding acquisition:** Michael Schindelegger
**Investigation:** Michael Schindelegger, Daniel P. Kotzian, Richard D. Ray
**Methodology:** Michael Schindelegger, Richard D. Ray, J. A. Mattias Green
**Resources:** Michael Schindelegger



**Abstract** The Gulf of Maine's lunar semidiurnal ($M_2$) ocean tide exhibits spatially coherent amplitude changes of ∼1–3 cm on interannual time scales, though no causative mechanism has been identified. Here we show, using a specially designed numerical modeling framework, that stratification changes account for 32%–48% (Pearson coefficient 0.58–0.69) of the observed $M_2$ variability at tide gauges from 1994 to 2019. Masking experiments and energy diagnoses reveal that the modeled variability is primarily driven by fluctuations in barotropic-to-baroclinic energy conversion on the continental slope south of the gulf's mouth, with a 1-cm amplitude increase at Boston corresponding to a ∼7% (0.30 GW) drop in the area-integrated conversion rate. Evidence is given for the same process to have caused the decade-long $M_2$ amplitude decrease in the Gulf of Maine beginning in 1980/81. The study has implications for nuisance flooding predictions and space geodetic analyses seeking highest accuracies.

**Plain Language Summary** The height of the twice-daily tide at Boston is about 135 cm, but researchers have long noted that this value fluctuates by about 1–3 cm from year to year. Here we show that the annual tidal height changes—seen in fact throughout the Gulf of Maine—are closely linked to how seawater density is distributed three-dimensionally in the region. In particular, as tidal currents enter the gulf over steep underwater topography, the vertical distribution of density determines how much of the incoming wave energy is scattered back as internal tides into the deeper Northwest Atlantic. In years where this conversion of wave energy drops by 7% from its nominal value of 4 Gigawatt, the surface tide at Boston typically increases by 1 cm. Climate-induced changes in ocean temperature and density may strengthen or weaken the conversion effect and thus slightly alter the role of tides in coastal flood events.

## 1. Introduction

The tides of the Gulf of Maine and Bay of Fundy (BF) are remarkable not only for their large amplitudes but also for their large changes: a secular increase in the $M_2$ amplitude has been ongoing since the early twentieth century (e.g., Godin, 1995; Greenberg et al., 2012; Ray, 2006; Ray & Talke, 2019). There is also significant interannual variability in $M_2$ of order 1–3 cm, again remarkable because it is coherent throughout the whole gulf. In fact, at all tide gauges north of Boston, the year-to-year changes are in near lockstep (Ray & Talke, 2019, Figure 3). Here we aim to unravel some of the mystery of these interannual changes, in part seeking clues as to what drives the tide's secular trend. Understanding the non-stationary behavior of $M_2$ may seem a quixotic endeavor at first sight, but it turns out to be important for nuisance flooding predictions (Baranes et al., 2020; Ray & Foster, 2016) and the de-aliasing of satellite gravimetry and altimetry observations (e.g., Flechtner et al., 2016). In particular, the continental slope south of Browns Bank (Figure 1a) is one of the few locations where satellite-derived western boundary pressures might be used (in future) to determine North Atlantic meridional transport variability (Bentel et al., 2015; Hughes et al., 2018). The relevant bottom pressure signals are very small (±1 mbar) and could easily be corrupted by spatially and temporally aliased tide model errors. Moreover, if variability in $M_2$ concerns—apart from the gulf's barotropic tide—the surface signature of open-ocean internal tides, that would be of relevance for the submesoscale analysis envisioned with the Surface Water Ocean Topography mission (SWOT, Arbic et al., 2015; Morrow et al., 2019).

Interannual sea level fluctuations are insufficient to explain the tidal amplitude changes measured at the coast (Greenberg et al., 2012; Ray & Talke, 2019; Schindelegger et al., 2018). On the other hand, there is a known cm-level sensitivity of tidal elevations inside the gulf to seasonal changes in ocean stratification (Chen et al., 2011;

**Software:** Michael Schindelegger, Daniel P. Kotzian
**Supervision:** Michael Schindelegger, J. A. Mattias Green, Sophie Stolzenberger
**Validation:** Michael Schindelegger, Richard D. Ray
**Visualization:** Michael Schindelegger
**Writing – original draft:** Michael Schindelegger
**Writing – review & editing:** Michael Schindelegger, Richard D. Ray, J. A. Mattias Green, Sophie Stolzenberger

Katavouta et al., 2016). Our main objective is thus to test whether the observed year-to-year changes in $M_2$ (since 1993) likewise arise from variations in ocean stratification and to determine where such changes are most effective and by what mechanism. Section 2 introduces our numerical modeling approach, before pertinent aspects of the region's tidal dynamics are described in Section 3. Results on interannual $M_2$ variability (Section 4) are complemented by a brief look at implications for lower-frequency amplitude changes in Section 5.

## 2. Methods and Data

### 2.1. Tide Gauges

Hourly water level data at stations Eastport, Bar Harbor, Portland, and Boston (Figure 1a) form the observational basis for this work. Measurements were collected by NOAA (U.S. National Oceanic and Atmospheric Administration) and extracted by us from the GESLA-3 (Global Extreme Sea Level Analysis Version 3, Haigh et al., 2022) database. We ignore observations from St. John in the BF, as the tide gauge was relocated in 1999 (Ray & Talke, 2019). Records were partitioned into yearly segments and tidally analyzed for 67 constituents, with standard errors deduced from scaled colored residual spectra (Codiga, 2011). The resultant time series of annual $M_2$ harmonics extend well into the first half of the 20th century and are dominated by the 18.6-year nodal modulation. A weighted least-squares fit was applied to remove the 18.6-year term (but no higher harmonic given the lack of evidence in spectra), before the annual estimates were curtailed to the period of interest (1993–2019). The Bar Harbor series is affected by a data gap from 1999 to 2001 and is therefore secondary to our presentation below.

### 2.2. Numerical Model

Our modeling framework is the MITgcm (Massachusetts Institute of Technology general circulation model, Marshall et al., 1997), which has been used in numerous regional studies of tidal dynamics and internal waves (e.g., Buijsman et al., 2012; Ponte & Cornuelle, 2013; Zeng et al., 2021). The central part of our three-dimensional (3D) computational domain, depicted in Figure 1a, is a 6°20′ × 8°20′ latitude-longitude patch covering the wider Gulf of Maine area with a grid spacing of 2′ (arcmin), or equivalently, ∼2.7 × 3.7 km. Away from the southern (39°20′ N) and eastern (62°50′ W) limits of the central domain, grid cells are gradually stretched to reach a maximum spacing of 11′ at the open model boundaries in the South (31°36′ N) and East (55°4′ W). For stability reasons, we adopt a linear free surface and classical $z$ coordinates. Vertical resolution increases from 6 m in the upper 40 m of the ocean to 457 m at depth, totaling 57 layers. Bathymetry is based on the 30-arcsec RTopo-2 Data set (Schaffer et al., 2016), and topographic variability in between layer mid-points is represented by a partial cell formulation (Adcroft et al., 1997).

We conduct separate simulations for individual time slices, representing single years from 1993 to 2019, or months of the seasonal cycle. Each simulation is started from rest and taken to 20 days under identical forcing, consisting of along- and cross-boundary currents with a 3-day ramp up to full strength. The transports are a superposition of $M_2$ barotropic velocities (taken from the TPXO9-atlas of Egbert & Erofeeva, 2002, updated version) and steady-state geostrophic currents consistent with the hydrography of the region. Use of a 4-point sponge layer with a short relaxation time scale (∼1,000 s, Ponte & Cornuelle, 2013), along with the large size of the modeling domain, render the influence of wave reflections on the interior solution negligible. Our setup neither considers nodal variations in tidal boundary conditions nor atmospheric forcing. Similarly, equilibrium tidal forcing is omitted, as it has no appreciable impact on the results presented below.

Perturbations of the $M_2$ tide are induced by exchanging the model's initial potential temperature ($\theta$) and salinity ($S$) fields from simulation to simulation (cf. Kang et al., 2002; Zaron & Egbert, 2014). We interpolate the respective ($\theta$, $S$) fields in 3D from a high-resolution 1/12° global ocean reanalysis (GLORYS12 Version 1, Lellouche et al., 2018), covering the period 1993–2019 at this writing. GLORYS12 uses a reduced-order Kalman filter to constrain an eddy-resolving ocean model to many observations, including along-track altimetry, satellite sea surface temperature, hydrographic sections, XBT, and Argo (Szekely et al., 2016). We average the reanalyzed ($\theta$, $S$) fields into a 1993–2019 mean climatology for the control run and into annual means and calendar month composites for the perturbation experiments. The stratification changes are restricted to the central modeling domain and transition linearly to the control run climatology over a 1° buffer zone. To avoid drifts of isopycnal

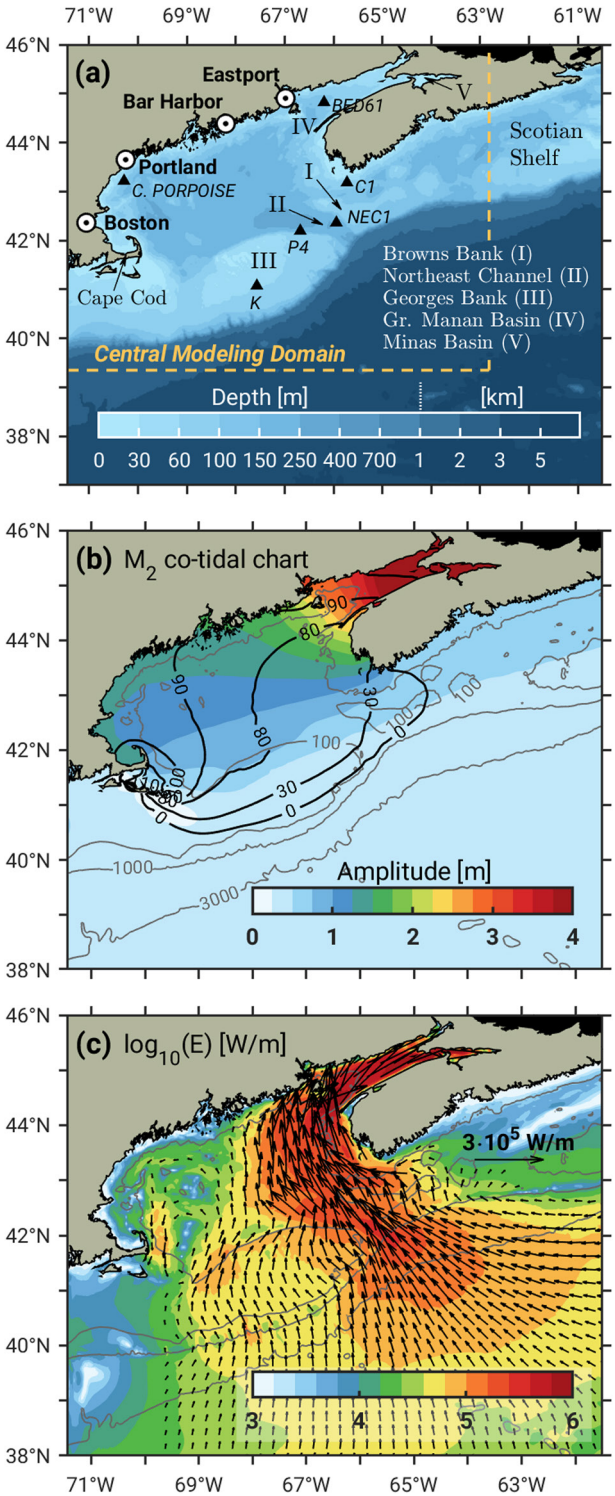


**Figure 1.** (a) Model bathymetry, geographical names, and utilized sites with observational data (circles for tide gauges, triangles for moorings). (b) $M_2$ co-tidal chart of the control run, with Greenwich phase lags (deg) plotted as black isolines. (c) Total $M_2$ energy flux vectors, **E** (see Supporting Information S1) of the control run, averaged in 1/4° boxes, with magnitudes indicated by colored contours on log-scale.

surfaces during integration, we constrain the $(\theta, S)$ fields to initial values at each 3D location, using a relaxation time scale of 2.5 days.

In choosing the vertical mixing scheme, we required that the model captures the $M_2$ seasonal cycle in elevation, which has been linked to turbulent energy losses, for example, on top of Georges Bank (Katavouta et al., 2016). Vertical eddy viscosities $\nu$ and diffusivities are thus computed via the $K$-profile parameterization of Large et al. (1994). For the ocean interior, that is, below the mixed layer, $\nu$ contains contributions from shear instability and internal wave breaking, specified as a constant background viscosity ($\nu_b = 5\ 10^{-5}\ m^2\ s^{-1}$) in the momentum equations. We use a modified Leith scheme (Fox-Kemper & Menemenlis, 2008) for horizontal viscosity, while quadratic bottom drag is prescribed with a non-dimensional coefficient of 0.003.

## 3. Selected Tidal Characteristics

The co-tidal elevation chart and $M_2$ total energy flux vectors (**E**) from the control run (Figures 1b and 1c) illustrate the familiar characteristics of the area's lunar semidiurnal oscillation. Tidal power from the deep ocean enters the resonant system over the Western Scotian Shelf, the Northeast Channel, and via cross-isobath flow on Georges Bank (cf. Chen et al., 2011). Inside the gulf, the energy flux divides into a branch directed up the BF and a (weak) counterclockwise component propagating westward and ultimately southward to Cape Cod with an amplitude ($H$) of about 1.3 m. Greenwich phase values ($G$) increase from 80° to approximately 105° after separation into the two branches, with later appearance of the tide ($G$ ~135°) seen in the Minas Basin. Figure 1b also depicts the characteristic amplitude growth to above 4 m in the BF, accompanied by total energy fluxes in excess of 5 $10^5$ W $m^{-1}$. Simulations with seasonally varying density structures suggest that $M_2$ attains its maximum amplitude in March/April and its minimum in October throughout the Gulf of Maine in the model (Figure S2 in Supporting Information S1). Spring-autumn differences are largest in the upper reaches of the BF (13 cm) and flatten out to 3.5 cm along the Massachusetts coast. Superimposed on the broad pattern of amplitude changes in the gulf's interior are internal tide signatures emanating from the northern flank of Georges Bank (Katavouta et al., 2016), particularly in stratified conditions from May to October (Li et al., 2015).

Validation efforts (Table 1) suggest that modeled tidal constants ($H$, $G$) are consistent with estimates at the four tide gauges, to within 12° or better for phase lags. Amplitudes transition from being too small by 4–7 cm in the western Gulf of Maine into an overestimation of 10 cm at Eastport; the excess amplitude at St. John would be 36 cm, or 12% in relative terms. Taking spatial averages over the central modeling domain plus 1° buffer, the $M_2$ solution of the control run has a root mean square elevation error relative to TPXO9 of 13.2 cm, split in equal portions into amplitude (9.2 cm) and phase (9.0 cm) errors. Comparisons with observed $M_2$ tidal current ellipses at six locations (Figures 1a, Moody et al., 1984) and various depths are shown in Figure S1 in Supporting Information S1. Evidently, the model produces a realistic 3D tidal state, although currents speeds are somewhat too large at most locations. Turning again to elevations, seasonal changes in $M_2$ amplitude deduced from monthly response analyses at the four tide gauges (Ray & Talke, 2019) agree reasonably well with simulation results (Figure S3 in Supporting Information S1). Spring amplitudes plateau by 1–2 months too early in the model, but these are minor distortions compared to what we found in runs with other

**Table 1**
*Evaluation of Simulation Results at Tide Gauges*[a,b]

| | $H$ (cm) | | $G$ (°) | | | |
|---|---|---|---|---|---|---|
| Station | Model | obs. | Model | obs. | $R$ | PVE (%) |
| Eastport | 276 | 266 | 100 | 99 | 0.58 (0.49) | 32 (21) |
| Bar harbor | 157 | 158 | 88 | 93 | 0.64 (0.50) | 41 (24) |
| Portland | 133 | 137 | 93 | 103 | 0.64 (0.51) | 41 (25) |
| Boston | 131 | 138 | 98 | 110 | 0.69 (0.53) | 48 (25) |

[a]Observed amplitudes $H$ and phase lags $G$, used for validating the $M_2$ control run, are 1993–2019 averages, while statistics for interannual variability (correlation $R$ and percentage variance explained PVE) are given both for 1993–2019 (in parentheses) and 1994–2019; see discussion in Section 4. [b]As for $R$, $p$-values are 0.01 save Eastport (0.02), and effective degrees of freedom vary from 15 to 21.

vertical mixing schemes. We conclude that the model provides a sufficiently accurate description of the region's $M_2$ tide, though refinements (cf. Chen et al., 2011) are possible.

Figure 2 additionally illustrates baroclinic tidal fields, comprising depth-integrated semidiurnal baroclinic energy flux vectors, **F** (Nash et al., 2005; Vic et al., 2018), isopycnal excursions, and surface displacements of the stationary $M_2$ internal tide. A narrow beam of high flux values ($\geq 10^4$ W m$^{-1}$), directed from the gulf's mouth to the southeast, points to constructive interference of internal tides generated along a stretch of strong barotropic cross-isobath flow (Figure 1c). In-phase and quadrature parts of the baroclinic tidal surface variation attain maximum amplitudes of ∼4 cm, somewhat larger than their low-mode expression in empirical mapping results (Ray & Zaron, 2016). Wave propagation into the ocean interior, depicted in Figure 2c for the transect $\overline{\mathrm{AB}}$, is along gradually descending isopycnal surfaces of the background state, at depths of the permanent thermocline (200–1,000 m). Modeling work (e.g., Duda et al., 2018) suggests that the southbound internal tide may also interact with low-frequency currents embedded in the Gulf stream, but these offshore aspects of wave propagation are not germane to our study. To map internal tide generation sites more clearly, we have diagnosed the barotropic-to-baroclinic energy conversion rate ($C$) in the model (Buijsman et al., 2012; Kelly & Nash, 2010)

$$C \approx -\left\langle \nabla h \cdot \mathbf{U}(t) p_b'(t) \right\rangle \quad \left[\mathrm{W\ m^{-2}}\right] \tag{1}$$

where $h$ is the resting water depth, $\nabla h$ represents bathymetric slopes in eastward and northward direction, $\mathbf{U} = (U, V)$ is the barotropic tidal current, $p_b'$ is the bottom pressure anomaly due to internal tides, and angle brackets indicate time ($t$) averaging over multiple $M_2$ cycles. Mathematical expressions for **F** and the baroclinic pressure $p'$ are given in Supporting Information S1.

Figure 2b shows that the conversion of tidal energy is strongly focused over a ∼2°-long continental slope section centered around the mouth of the Northeast Channel. Peak conversion rates (2–3 W m$^{-2}$) occur just off the southern tip of Browns Bank at a depth of ∼350 m, with more widespread values of $C$ in the range of 0.1–1 W m$^{-2}$ encased by the 150-m and 1,000-m isobaths. We find localized secondary maxima of tidal conversion in the Grand Manan Basin, on the northeast flank of Georges Bank, and in the submarine canyons at the shelf break near 40°N. Areas where $C$ is a sink for baroclinic tidal energy do exist (e.g., near 2,000 m on the continental slope where $p_b'$ and **U** are out of phase), but these features are weak enough ($C \leq 0.05$ W m$^{-2}$) to warrant their being clipped in Figure 2b. The net barotropic-to-baroclinic $M_2$ energy transfer $\overline{C}$, integrated over the entire model domain, is 3.95 GW in the control run, including a small contribution from sinks (−0.49 GW). For comparison, a repeat of the 57-layer simulation on a 1.5′ horizontal grid gave $\overline{C} = 4.06$ GW, suggesting that the domain-integrated conversion deduced from Figure 2b is probably a lower bound.

## 4. Interannual Variability

We are now poised for insight into the variability of $M_2$ on interannual time scales. Modeled amplitude changes ($\Delta H$) at three ports (Figure 3a), along with the spatial pattern of $\Delta H$ in three selected years (Figures 2d–2f) demonstrate a subtle yet clear dependence of the Gulf of Maine tide to changes in the region's annual mean stratification. The signal interior to the gulf increases from somewhat less than 1 cm in more anomalous years (e.g., 2007 and 2012) to twice that value at Eastport and up to 3 cm in the central BF. These series contain a very small contribution from water column thickness (i.e., relative sea level) changes, as the steric expansion in the model varies with the adopted density structure. Largest year-to-year fluctuations in steric height amount to 3–4 cm throughout the gulf and several dm in the abyssal ocean (not shown). We have imposed these patterns as bathymetry perturbations in global barotropic tide simulations (cf. Schindelegger et al., 2018) to place upper bounds on the impact of interannual sea level changes on the amplitudes of $M_2$. Reasonable estimates are ≲2 mm at Eastport and ≲0.5 mm in the western Gulf of Maine, in accord with simple scalings based on Figure 7 in Haigh et al. (2020).

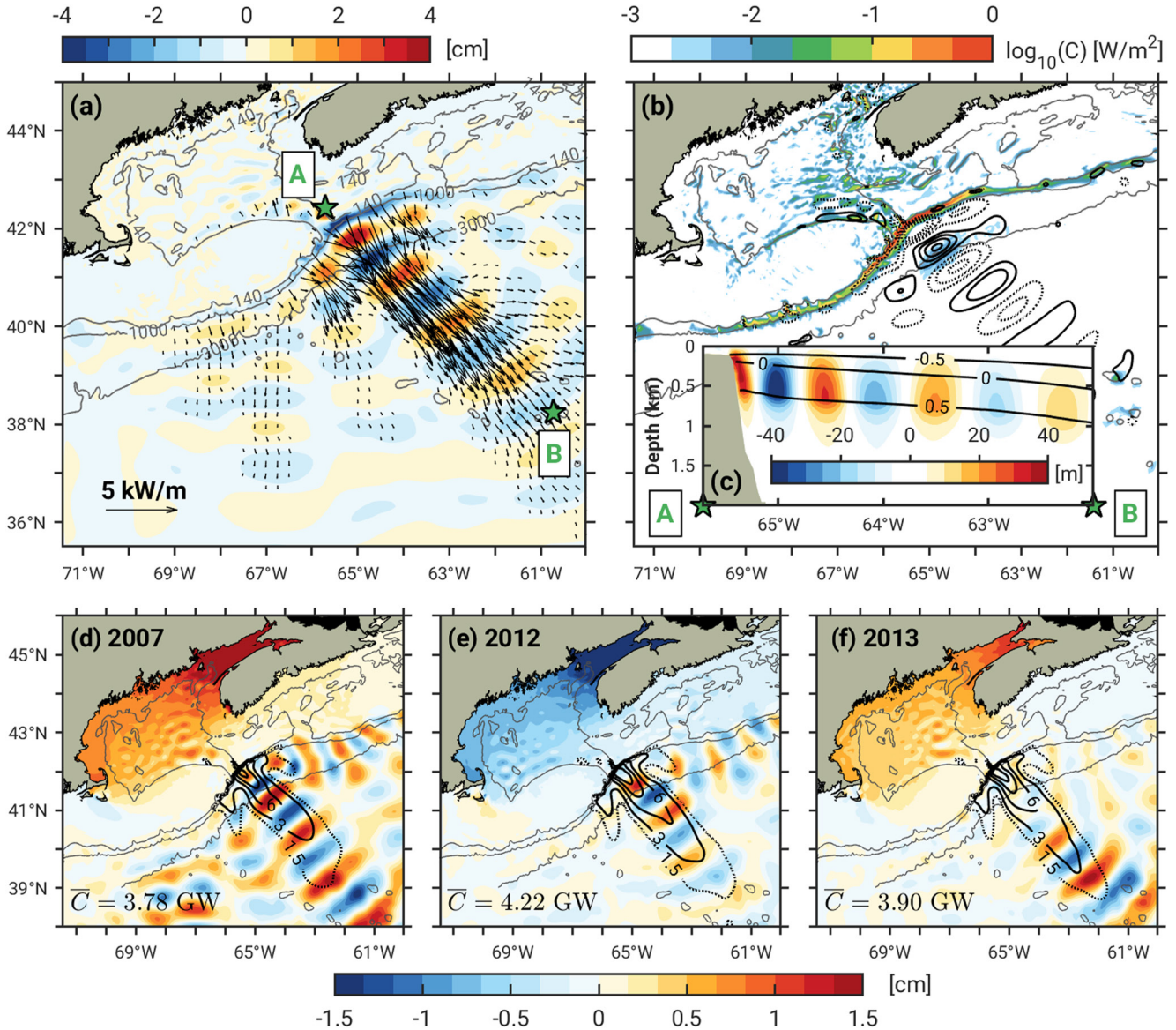


**Figure 2.** (a) Stationary $M_2$ internal tide in surface elevation (in-phase part), overlain by baroclinic energy flux vectors **F**, averaged to a 1/4° grid and clipped if <0.2 kW m$^{-1}$. (b) Barotropic-to-baroclinic $M_2$ conversion rates $C$ (color shading on log-scale) and quadrature part of the stationary internal tide, drawn as black contours in intervals from ±1 to ±4 cm, with negative values shown as dashed lines. (c) In-phase component of vertical isopycnal excursion (defined as in Gerkema & van Haren, 2007, color shading), plotted along the transect $\overline{AB}$ (see panel a). Shown atop are contours of background potential density anomalies relative to a value of 1,027 kg m$^{-3}$. All fields in (a–c) pertain to the control simulation. Panels (d–f) depict $M_2$ amplitude changes in elevation for the years 2007, 2012, and 2013 (color shading), relative to the control run, while black contours mark the magnitude of **F** in intervals from 1.5 to 12 kW m$^{-1}$. The respective area-integrated conversion rate $\overline{C}$ is given in the bottom left corner. Figure S4 in Supporting Information S1 shows analogous maps for 12 other years.

Figure 3a contains more findings of value. Specifically, the timing and magnitude of the simulated amplitude changes are broadly consistent with observations, featuring periods of both close agreement (e.g., 1994–1999) and larger disparities (e.g., 2002–2005). Although correlations remain high, the more erratic tidal variations after 2012 are less reliably captured the closer the proximity to the BF. During 1993–2019, the percentage of observed $M_2$ variance accounted for by the model is $\lesssim$25% (Table 1), but close examination of the time series reveals that these statistics are unduly influenced by conditions in a single year (1993). Masking experiments (see below and red curves in Figure 3a) suggest that the simulated amplitude decrease in 1993 is a doubtful peculiarity originating from the BF, possibly reflecting shortcomings in the early GLORYS12 data or the vertical mixing scheme. It is thus not unreasonable to omit 1993 from the quantitative model-data comparison in Table 1. From 1994 to

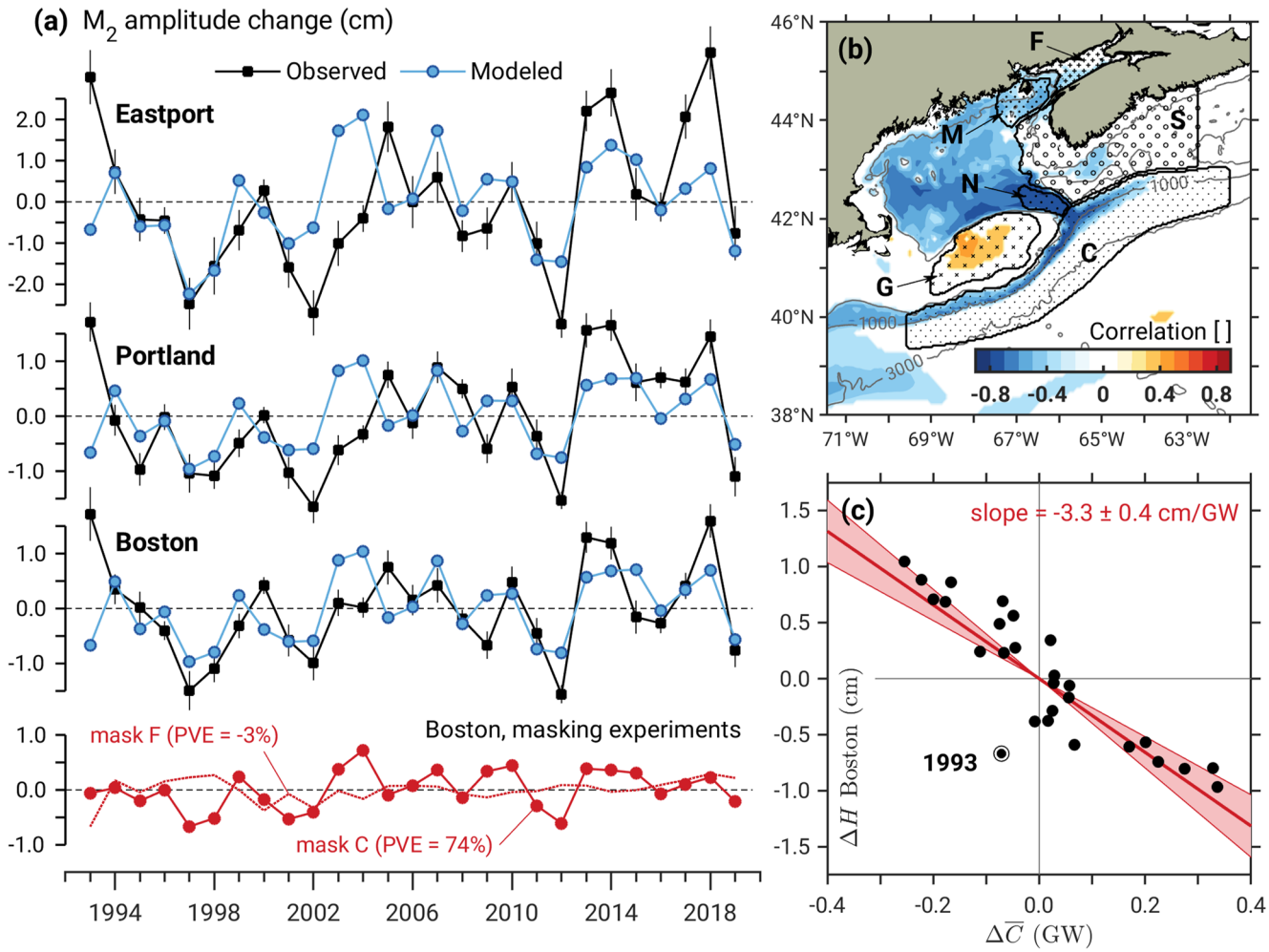


**Figure 3.** (a) Annual $M_2$ amplitude changes ($\Delta H$, in cm) from 1993 to 2019 at three ports from observations (black markers, with standard errors) and simulations (blue markers). Red curves on the bottom axes show simulated amplitude variations at Boston with stratification changes restricted either to the continental slope (mask C) or to the Bay of Fundy (mask F). Stippled patches in (b) illustrate the placement of all masks, underlain by colored contours for the correlation between modeled $\Delta H$ at Boston and time series (1993–2019) of the potential energy anomaly change $\Delta\phi$ from GLORYS12. Correlations with $p > 0.10$ have been masked. Panel (c) regresses the Boston $\Delta H$ from simulations against annual changes in the domain-integrated $M_2$ tidal conversion rate, $\overline{C}$, relative to the control run value of 3.95 GW. The red curve is a straight line fit to these anomalies, with estimated uncertainties (95% confidence level) represented by the shaded area.

2019, we find explained variances between 32% at Eastport and 41%–48% in the western Gulf of Maine, with Pearson's $R$ reaching a maximum of 0.69 at Boston.

The link of interannual tidal changes at the coast to stratification is engaging and raises the question as to what region and physical mechanism(s) form the root cause of these signals. Examination of $\Delta H$ in relation to a space-time distribution of the potential energy anomaly $\phi$ (Simpson, 1981)

$$\phi = \frac{1}{h}\int_{-h}^{0} \tilde{\rho}(z) g z \, \mathrm{d}z \quad \left[\mathrm{J\ m^{-3}}\right] \tag{2}$$

may provide a clue. Here, $z$ is the vertical coordinate (positive upwards), $g$ is the gravitational acceleration, and $\tilde{\rho}$ denotes the deviation of the (background) potential density $\rho$ from its vertical average. Figure 3b illustrates the correlation between simulated $M_2$ amplitude changes at Boston and temporal variations in $\phi$ ($\Delta\phi$, relative to a 1993–2019 average), calculated from the yearly GLORYS12 fields for initial hydrography. The map features an area of moderate positive correlation on Georges Bank, which likely portends a mixing effect; in particular, increased stability of the water column (positive $\Delta\phi$) reduces vertical eddy viscosity and the implied turbulent dissipation, thus allowing for higher amplitudes across the basin. Negative correlations in the central gulf and

BF are somewhat more puzzling but might mean that here, higher velocities and velocity shear in stratified conditions increases turbulent energy losses in the bottom boundary layer (Müller, 2012). Yet most attention in Figure 3b is drawn to significant negative correlations ($-0.85 \leq R \leq -0.65$) over the Northeast Channel and the adjacent continental slope. Could there be a teleconnection between tidal dynamics at the mouth of the gulf and the modeled $M_2$ variability at the coast?

Figures 2d–2f strengthens the case for this. In 2012, decreased tidal amplitudes throughout the gulf coincide with a comparatively large net barotropic-to-baroclinic conversion rate ($\overline{C} = 4.22$ GW) and enhanced fluxes into the internal tide generated at the shelf break. The reverse is true in years of positive $\Delta H$ (e.g., 2007), and several more experiments (e.g., 1997–1999, Figure S4 in Supporting Information S1) confirm these observations. For a condensed view of the matter, we regress modeled $\Delta H$ at Boston against annual fluctuations in the domain-integrated conversion rate (Figure 3c). The correlation is striking ($R = -0.88$), and most points follow a straight line with a slope of $-3.3 \pm 0.4$ (units are cm GW$^{-1}$). We find a nearly identical slope at Portland ($-3.2 \pm 0.3$) and twice that value at Eastport ($-6.5 \pm 0.5$). The estimates are largely governed by tidal conversion changes on the continental slope, given that this region accounts for 78% of the interannual variance in domain-wide $\overline{C}$.

To substantiate the evidence, we repeated the yearly perturbation experiments a total of six times, each time restricting the stratification changes to a particular region, while adopting the control run $(\theta, S)$ elsewhere. These masks extend across all vertical layers, with their horizontal limits marked out in Figure 3b. Care was exercised in choosing the southern bound of mask C on the continental slope, as the characteristic internal wave field and tidal conversion of a year only develop if the stratification changes cover a wide enough area. We found a meridional extent of approximately one internal tide wavelength of the main tidal beam (Figure 2a) to be a sensible choice. Statistics in Table S1 (Supporting Information S1) confirm that coastal $\Delta H$ signals in the yearly simulations ("no mask") are indeed mainly associated with changes in the offshore energy transfer into baroclinic tides. The percentage of "no mask" variance attributed to the continental slope is 69%–75%, and as high as 83% over 1995–2012; cf. Figure 3a. Secondary contributions arise from the Western Scotian Shelf (mask S), either due to small-scale conversion effects or turbulent energy losses as the tide rotates into the BF (Chen et al., 2011). The impact of all other regions, including Georges Bank, is small, although Eastport exhibits a slightly enhanced sensitivity to stratification variability in the nearby Grand Manan Basin.

## 5. Conclusions

The unusual temporal evolution of $M_2$ in the Gulf of Maine has occupied researchers' attention time and again (e.g., Doodson, 1924; Godin, 1995; Greenberg et al., 2012; Ray, 2006; Ray & Talke, 2019). Here we have made a first more serious connection of parts of these changes with baroclinic tidal dynamics and density structures offshore. The model-data agreement we report is understandably imperfect, given that neither the GLORYS12 fields nor the numerical model are free from error. Evidently, a repeat of our simulations with geometrically more flexible finite element methods (Chen et al., 2011) and a wider range of vertical mixing schemes would help clarify further questions, including the role of stratification changes in the BF or sensitivities of $\overline{C}$ to topographic resolution.

We close with a remark on how our argument for the drivers of interannual $M_2$ variability can also explain tidal changes in the Gulf of Maine on longer timescales, for example, the near-monotonic $M_2$ decrease in amplitude from the early 1980s through 1991 (Müller, 2011). An origin for this amplitude shift in tidal energy conversion requires that stratification off the shelf break strengthened markedly over the same period (cf. Figure 3b). Indeed, potential energy anomalies, inferred from a 1/10° decadal hydrographic atlas (Seidov et al., 2016), increased by $\sim$100 J m$^{-3}$ from 1975 to 1984 to 1985–1994 over the relevant continental slope section south of the Northeast Channel (Figure S5 in Supporting Information S1). Using linear regression coefficients $\Delta H/\Delta\phi$ drawn from our yearly simulations, we estimate an implied $M_2$ change at Boston of $-1$ cm between 1975–1984 and 1985–1994, consistent with the observations. Strengthening of stratification during the 1980s was likely linked to upper-ocean warming at the entrance to the gulf (Figure 8b in Seidov et al., 2021), involving partial retreat of the Labrador Current in favor of warmer slope water from the Gulf Stream extension region. The process is projected to intensify with ongoing climate change (Saba et al., 2016) and could well mean that in coming decades, we might see decreasing instead of increasing $M_2$ amplitudes in the Gulf of Maine. Explicit numerical simulations of the type presented here will shed better light on this intriguing question.

## Data Availability Statement

The datasets used in this study are available from the following links: GESLA-3 tide gauge records (https://www.gesla.org/), TPXO9-atlas (https://www.tpxo.net/global/tpxo9-atlas), RTopo-2 (https://doi.pangaea.de/10.1594/PANGAEA.856844), GLORYS12 Version 1 (https://marine.copernicus.eu/access-data, product identifier GLOBAL_MULTIYEAR_PHY_001_030), and Seidov et al. (2016) decadal climatologies (https://www.ncei.noaa.gov/products/northwest-atlantic-regional-climatology). The MITgcm setutp and input files to reproduce our yearly simulations are provided in Schindelegger and Kotzian (2022).

**Acknowledgments**
We thank two anonymous reviewers for their suggestions. This work was supported by the German Research Foundation (DFG, Project no. 451039647) and the Austrian Science Fund (FWF, Grant P30097-N29). We gratefully acknowledge the Gauss Centre for Supercomputing e.V. (www.gauss-centre.eu) for funding this project by providing computing time through the John von Neumann Institute for Computing (NIC) on the GCS Supercomputer JUWELS at Jülich Supercomputing Centre (JSC). Open Access funding enabled and organized by Projekt DEAL.

## References

Adcroft, A., Hill, C., & Marshall, J. (1997). Representation of topography by shaved cells in a height coordinate ocean model. *Monthly Weather Review*, *125*(9), 2293–2315. https://doi.org/10.1175/1520-0493(1997)125⟨2293:ROTBSC⟩2.0.CO;2

Arbic, B. K., Lyard, F., Ponte, A., Ray, R. D., Richman, J. G., Shriver, J. F., et al. (2015). Tides and the SWOT mission: Transition from science definition team to science team. *Civil and Environmental Engineering Faculty Publications and Presentations*, *336*, 1–8.

Baranes, H. E., Woodruff, J. D., Talke, S. A., Kopp, R. E., Ray, R. D., & DeConto, R. M. (2020). Tidally driven interannual variation in extreme sea level frequencies in the Gulf of Maine. *Journal of Geophysical Research: Oceans*, *125*(10), e2020JC016291. https://doi.org/10.1029/2020JC016291

Bentel, K., Landerer, F. W., & Boening, C. (2015). Monitoring Atlantic overturning circulation and transport variability with GRACE-type ocean bottom pressure observations—A sensitivity study. *Ocean Science*, *11*(6), 953–963. https://doi.org/10.5194/os-11-953-2015

Buijsman, M. C., Legg, S., & Klymak, J. (2012). Double-ridge internal tide interference and its effect on dissipation in Luzon Strait. *Journal of Physical Oceanography*, *42*(8), 1337–1356. https://doi.org/10.1175/JPO-D-11-0210.1

Chen, C., Huang, H., Beardsley, R. C., Xu, Q., Limeburner, R., Cowles, G. W., et al. (2011). Tidal dynamics in the Gulf of Maine and New England Shelf: An application of FVCOM. *Journal of Geophysical Research*, *116*(C12), C12010. https://doi.org/10.1029/2011JC007054

Codiga, D. L. (2011). *Unified tidal analysis and prediction using the UTide Matlab functions (Tech. Rep. No. 2011-01)*. Graduate School of Oceanography, University of Rhode Island Narragansett. https://doi.org/10.13140/RG.2.1.3761.2008

Doodson, A. T. (1924). Perturbations of harmonic tidal constants. *Proceedings of the Royal Society*, *106*(739), 513–526. https://doi.org/10.1098/rspa.1924.0085

Duda, T. F., Lin, Y.-T., Buijsman, M., & Newhall, A. E. (2018). Internal tidal modal ray refraction and energy ducting in baroclinic Gulf Stream currents. *Journal of Physical Oceanography*, *48*(9), 1969–1993. https://doi.org/10.1175/JPO-D-18-0031.1

Egbert, G. D., & Erofeeva, S. Y. (2002). Efficient inverse modeling of barotropic ocean tides. *Journal of Atmospheric and Oceanic Technology*, *19*(2), 183–204. https://doi.org/10.1175/1520-0426(2002)019⟨0183:EIMOBO⟩2.0.CO;2

Flechtner, F., Neumayer, K.-H., Dahle, C., Dobslaw, H., Fagiolini, E., Raimondo, J.-C., & Güntner, A. (2016). What can be expected from the GRACE-FO laser ranging interferometer for Earth science applications? *Surveys in Geophysics*, *37*(2), 453–470. https://doi.org/10.1007/s10712-015-9338-y

Fox-Kemper, B., & Menemenlis, D. (2008). Can large eddy simulation techniques improve mesoscale rich ocean models? In M. W. Hecht & H. Hasumi (Eds.), *Ocean modeling in an eddying regime* (pp. 319–337). American Geophysical Union (AGU). https://doi.org/10.1029/177GM19

Gerkema, T., & van Haren, H. (2007). Internal tides and energy fluxes over Great Meteor Seamount. *Ocean Science*, *3*(3), 441–449. https://doi.org/10.5194/os-3-441-2007

Godin, G. (1995). Rapid evolution of the tide in the Bay of Fundy. *Continental Shelf Research*, *15*(2), 369–372. https://doi.org/10.1016/0278-4343(93)E0005-S

Greenberg, D. A., Blanchard, W., Smith, B., & Barrow, E. (2012). Climate change, mean sea level and high tides in the Bay of Fundy. *Atmosphere-Ocean*, *50*(3), 261–276. https://doi.org/10.1080/07055900.2012.668670

Haigh, I. D., Marcos, M., Talke, S. A., Woodworth, P. L., Hunter, J. R., Hague, B. S., et al. (2022). GESLA version 3: A major update to the global higher-frequency sea-level data set. *Geoscience Data Journal*, *00*, 1–22. https://doi.org/10.1002/gdj3.174

Haigh, I. D., Pickering, M. D., Green, J. A. M., Arbic, B. K., Arns, A., Dangendorf, S., et al. (2020). The tides they are a-changin': A comprehensive review of past and future nonastronomical changes in tides, their driving mechanisms, and future implications. *Reviews of Geophysics*, *58*(1), e2018RG000636. https://doi.org/10.1029/2018RG000636

Hughes, C. W., Williams, J., Blaker, A., Coward, A., & Stepanov, V. (2018). A window on the deep ocean: The special value of ocean bottom pressure for monitoring the large-scale, deep-ocean circulation. *Progress in Oceanography*, *161*, 19–46. https://doi.org/10.1016/j.pocean.2018.01.011

Kang, S. K., Foreman, M. G. G., Lie, H.-J., Lee, J.-H., Cherniawsky, J., & Yum, K.-D. (2002). Two-layer tidal modeling of the Yellow and East China Seas with application to seasonal variability of the $M_2$ tide. *Journal of Geophysical Research*, *107*(C3), 3020. https://doi.org/10.1029/2001JC000838

Katavouta, A., Thompson, K. R., Lu, Y., & Loder, J. W. (2016). Interaction between the tidal and seasonal variability of the Gulf of Maine and Scotian shelf region. *Journal of Physical Oceanography*, *46*(11), 3279–3298. https://doi.org/10.1175/JPO-D-15-0091.1

Kelly, S. M., & Nash, J. D. (2010). Internal-tide generation and destruction by shoaling internal tides. *Geophysical Research Letters*, *37*(23), L23611. https://doi.org/10.1029/2010GL045598

Large, W. G., McWilliams, J. C., & Doney, S. C. (1994). Oceanic vertical mixing: A review and a model with a nonlocal boundary layer parameterization. *Reviews of Geophysics*, *32*(4), 363–403. https://doi.org/10.1029/94RG01872

Lellouche, J.-M., Greiner, E., Le Galloudec, O., Garric, G., Regnier, C., Drevillon, M., et al. (2018). Recent updates to the Copernicus Marine Service global ocean monitoring and forecasting real-time 1/12° high-resolution system. *Ocean Science*, *14*(5), 1093–1126. https://doi.org/10.5194/os-14-1093-2018

Li, Y., Fratantoni, P. S., Chen, C., Hare, J. A., Sun, Y., Beardsley, R. C., & Ji, R. (2015). Spatio-temporal patterns of stratification on the Northwest Atlantic shelf. *Progress in Oceanography*, *134*, 123–134. https://doi.org/10.1016/j.pocean.2015.01.003

Marshall, J., Adcroft, A., Hill, C., Perelman, L., & Heisey, C. (1997). A finite-volume, incompressible Navier Stokes model for studies of the ocean on parallel computers. *Journal of Geophysical Research*, *102*(C3), 5753–5766. https://doi.org/10.1029/96JC02775

Moody, J. A., Butman, B., Beardsley, R. C., Brown, W. S., Daifuku, P., Irish, J. D., et al. (1984). Atlas of tidal elevation and current observations on the Northeast American continental shelf and slope. *US Geological Survey Bulletin*, *1611*, 122. https://doi.org/10.3133/b1611

Morrow, R., Fu, L.-L., Ardhuin, F., Benkiran, M., Chapron, B., Cosme, E., et al. (2019). Global observations of fine-scale ocean surface topography with the Surface Water and Ocean Topography (SWOT) mission. *Frontiers in Marine Science*, *6*, 232. https://doi.org/10.3389/fmars.2019.00232

Müller, M. (2011). Rapid change in semi-diurnal tides in the North Atlantic since 1980. *Geophysical Research Letters*, *38*(11), L11602. https://doi.org/10.1029/2011GL047312

Müller, M. (2012). The influence of changing stratification conditions on barotropic tidal transport and its implications for seasonal and secular changes of tides. *Continental Shelf Research*, *47*, 107–118. https://doi.org/10.1016/j.csr.2012.07.003

Nash, J. D., Alford, M. H., & Kunze, E. (2005). Estimating internal wave energy fluxes in the ocean. *Journal of Atmospheric and Oceanic Technology*, *22*(10), 1551–1570. https://doi.org/10.1175/JTECH1784.1

Ponte, A. L., & Cornuelle, B. D. (2013). Coastal numerical modelling of tides: Sensitivity to domain size and remotely generated internal tide. *Ocean Modelling*, *62*, 17–26. https://doi.org/10.1016/j.ocemod.2012.11.007

Ray, R. D. (2006). Secular changes of the $M_2$ tide in the Gulf of Maine. *Continental Shelf Research*, *26*(3), 422–427. https://doi.org/10.1016/j.csr.2005.12.005

Ray, R. D., & Foster, G. (2016). Future nuisance flooding at Boston caused by astronomical tides alone. *Earth's Future*, *4*(12), 578–587. https://doi.org/10.1002/2016EF000423

Ray, R. D., & Talke, S. A. (2019). Nineteenth-century tides in the Gulf of Maine and implications for secular trends. *Journal of Geophysical Research: Oceans*, *124*(10), 7046–7067. https://doi.org/10.1029/2019JC015277

Ray, R. D., & Zaron, E. D. (2016). $M_2$ internal tides and their observed wavenumber spectra from satellite altimetry. *Journal of Physical Oceanography*, *46*(1), 3–22. https://doi.org/10.1175/JPO-D-15-0065.1

Saba, V. S., Griffies, S. M., Anderson, W. G., Winton, M., Alexander, M. A., Delworth, T. L., et al. (2016). Enhanced warming of the northwest Atlantic ocean under climate change. *Journal of Geophysical Research: Oceans*, *121*(1), 118–132. https://doi.org/10.1002/2015JC011346

Schaffer, J., Timmermann, R., Arndt, J. E., Kristensen, S. S., Mayer, C., Morlighem, M., & Steinhage, D. (2016). A global, high-resolution data set of ice sheet topography, cavity geometry, and ocean bathymetry. *Earth System Science Data*, *8*(2), 543–557. https://doi.org/10.5194/essd-8-543-2016

Schindelegger, M., Green, J. A. M., Wilmes, S.-B., & Haigh, I. D. (2018). Can we model the effect of observed sea level rise on tides? *Journal of Geophysical Research: Oceans*, *123*(7), 4593–4609. https://doi.org/10.1029/2018JC013959

Schindelegger, M., & Kotzian, D. (2022). *Numerical model of the semidiurnal ocean tide ($M_2$) in the Gulf of Maine*. Zenodo. https://doi.org/10.5281/zenodo.7181205

Seidov, D., Baranova, O. K., Boyer, T., Cross, S. L., Mishonov, A. V., & Parsons, A. R. (2016). Northwest Atlantic regional ocean climatology. In A. V. Mishonov (Ed.), *NOAA Atlas NESDIS 80, Tech*. Silver Spring, 56. https://doi.org/10.7289/V5/ATLAS-NESDIS-80

Seidov, D., Mishonov, A., & Parsons, R. (2021). Recent warming and decadal variability of Gulf of Maine and slope water. *Limnology & Oceanography*, *66*(9), 3472–3488. https://doi.org/10.1002/lno.11892

Simpson, J. H. (1981). The shelf-sea fronts: Implications of their existence and behaviour. *Philosophical Transactions of the Royal Society of London—Series A: Mathematical and Physical Sciences*, *302*(1472), 531–546. https://doi.org/10.1098/rsta.1981.0181

Szekely, T., Gourrion, J., Pouliquen, S., & Reverdin, G. (2016). CORA, Coriolis Ocean Dataset for Reanalyssis. *SEAONE*. https://doi.org/10.17882/46219

Vic, C., Naveira Garabato, A. C., Green, J. A. M., Spingys, C., Forryan, A., Zhao, Z., & Sharples, J. (2018). The lifecycle of semidiurnal internal tides over the northern Mid-Atlantic Ridge. *Journal of Physical Oceanography*, *48*(1), 61–80. https://doi.org/10.1175/JPO-D-17-0121.1

Zaron, E. D., & Egbert, G. D. (2014). Time-variable refraction of the internal tide at the Hawaiian Ridge. *Journal of Physical Oceanography*, *44*(2), 538–557. https://doi.org/10.1175/JPO-D-12-0238.1

Zeng, Z., Brandt, P., Lamb, K. G., Greatbatch, R. J., Dengler, M., Claus, M., & Chen, X. (2021). Three-dimensional numerical simulations of internal tides in the Angolan upwelling region. *Journal of Geophysical Research: Oceans*, *126*(2), e2020JC016460. https://doi.org/10.1029/2020JC016460